Published in final edited form as:
J Memb Sci. 2009 January 20; 326(2): 460–471. doi:10.1016/j.memsci.2008.10.025.

Thiol Functionalized Silica-Mixed Matrix Membranes for Silver Capture from Aqueous Solutions: Experimental Results and Modeling

A. R. Ladhe[1], **P. Frailie**[1], **D. Hua**[2], **M. Darsillo**[2], and **D. Bhattacharyya**[1,*]

[1]Department of Chemical and Materials Engineering, University of Kentucky, Lexington, KY 40506-0046

[2]J. M. Huber Corporation, Havre de Grace, MD

Abstract

The study deals with an aqueous phase application of Mixed Matrix Membranes (MMMs) for silver ion (Ag^+) capture. Silica particles were functionalized with 3-mercaptopropyltrimethoxy silane (MPTMS) to introduce free thiol (-SH) groups on the surface. The particles were used as the dispersed phase in the polysulfone or cellulose acetate polymer matrix. The membranes were prepared by the phase inversion method to create more open and interconnected porous structures suitable for liquid

* Corresponding author: D. Bhattacharyya, Alumni Professor, University of Kentucky, Phone: (859) 257-2794, Fax: (859) 323-1929, E-mail: db@engr.uky.edu.

List of symbols
A: Membrane water permeance (m/s.bar)
J_W: Membrane flux (m/s)
ΔP: Applied transmembrane pressure (bar)
W_1: Weight of wet membrane (kg)
W_2: Weight of dry membrane (kg)
ρ_W: Density of water (kg/m^3)
A_m: Membrane area (m^2)
L : Membrane thickness (m)
t_R : Residence time (s)
R: Dextran Rejection
r_S: Hydraulic radius of the dextran molecule (nm)
r_1: Hydrodynamic pore radius (nm)
M: Molecular weight of dextran (Da)
φ : Free volume fraction in membrane
φ_p: Polymer volume fraction in membrane
ρ_{Si}: Density of silica particles (kg/m^3)
ρ_p: Density of polysulfone (kg/m^3)
ψ: Weight fraction of silica in membrane
q' : Average composition of silica phase (moles of Ag^+/m^3 of silica Particles)
C' : Concentration of Ag^+ in bulk liquid phase (moles of Ag^+/m^3 of Liquid)
C_0: Inlet Ag^+ concentration ($mole/m^3$)
t' : Time (s)
z' : Distance down the membrane thickness (m)
γ : Equilibrium constant
k : Volumetric mass transfer coefficient (s^{-1})
C_0: Inlet feed concentration of silver ion ($mole/m^3$)
q_∞ : Maximum silver capture capacity (moles of silver/m^3 of silica)
T_S: Time at which saturation of silver capture was observed and experiment was terminated (s)

phase applications. The effects of the silica properties such as particle size, specific surface area, and porous/nonporous morphology on the silver ion capture capacity were studied. It was demonstrated that the membranes are capable of selectively capturing silver from a solution containing significant concentrations of other metal ions like Ca^{2+}. The membranes were studied to quantify the dynamic capacity for silver ion capture and its dependence on residence time through the adjustment of transmembrane pressure. The thiol-Ag^{+} interaction was quantified with Quartz Crystal Microbalance in a continuous flow mode experiment and the observations were compared with the membrane results. One dimensional unsteady state model with overall volumetric mass transfer coefficient was developed and solved to predict the silver concentration in the liquid phase and the solid silica phase along the membrane thickness at varying time. The breakthrough data predicted using the model is comparable with the experimental observations. The study demonstrates successful application of the functionalized silica-mixed matrix membranes for selective aqueous phase Ag^{+} capture with high capacity at low transmembrane pressures. The technique can be easily extended to other applications by altering the functionalized groups on the silica particles.

Keywords

Mixed matrix membrane; Thiol-silver interaction; Silica; Breakthrough curves; Quartz Crystal Microbalance; Unsteady state model

1. Introduction

Mixed matrix membranes (MMMs), which consist of a continuous polymeric phase and a dispersed inorganic particle phase (porous or non-porous), have been receiving increasing attention in the field of gas separations [1,2]. Many studies have demonstrated higher gas permeability and/or selectivity for the MMMs when compared to the conventional homogeneous polymeric membranes with working principle based on the solution-diffusion mechanism [3-6]. These membranes are shown to exceed Robeson's upper – bound limit [7] for the performance of polymeric membranes in gas separation. Inorganic materials have shown performances well beyond the upper bound, but their applications are hindered due to the difficulty in preparing defect free and economical inorganic membranes. MMMs combine the performance benefit of the inorganic membranes with the easy applicability benefit of the polymeric membrane.

Typically, MMMs have been prepared by casting a solution of polymer and dispersed inorganic phase, and then evaporating the solvent in a controlled environment to obtain a dense membrane. The choice of the polymer, inorganic phase, solvent, particle loading, and evaporation time are some of the important parameters affecting the morphology and performance of the MMMs.

Apart from the gas separation applications, the concept of such composite membranes is successfully applied in the case of barrier membranes, which are useful for food packaging and corrosion resistive coatings [8-10]. In this case the goal was to reduce the transport through the membranes, and it was accomplished either by adding impermeable flakes to the membrane polymer or by incorporating reactive groups within the membranes.

The important advantages of the MMMs in the gas separations have provoked little interest until now for extension of this concept to liquid phase separations. Researchers have reported MMMs applications for pervaporation to dehydrate organic mixtures [11-13]. Also the sulfonated silica-MMMs have been studied for fuel cell applications due to their improved proton conductivity, higher stability, and better performance [14-16]. Avramescu et al. [17] for the first time demonstrated the use of ion exchange-polymeric MMMs for adsorptive

biomolecule separation. The MMM adsorbers for enzyme capture and concentration have also been studied [18]. In order to change the membrane morphology from dense membrane (suitable in the case of gas separations) to more open micro-porous structure with high degree of pore interconnectivity (suitable for liquid phase applications), the MMMs were prepared via the well known phase inversion route with appropriate gelation bath temperature control. In this case it is desired to have a particle phase exhibiting rapid adsorption kinetics (for membrane adsorbers), high capacity and high selectivity towards target moiety, and easy regeneration. The MMMs have significant advantages over conventional column chromatography in terms of lower pressure drops, higher mass transfer rates (due to convective flow) resulting in higher throughputs, and easier scale-ups.

In our study, we applied the thiol functionalized MMMs for metal ion capture from aqueous salt solutions. Thiol functionalized systems have been studied extensively as metal ion adsorbents [19-27]. Vieira et al. [22] confirmed the preferential interaction of − SH groups with soft acids (Hg^{2+}>Ag^{+}>Cu^{2+}>Ni^{2+}>Zn^{2+}) in agreement with Pearson's concept [28] of hard and soft acids and bases. Kang et al. [21] demonstrated highly selective adsorption capacity of the thiol functionalized mesoporous silica materials for noble metal ions in the presence of other metal ions. Such a binding selectivity towards the target metal ions is important for many applications like waste treatment, which often involves metal ion mixtures.

Silver nitrate is a commonly used salt in many processes in the mirroring, photographic and electroplating industries [29]. Compared to most metals, silver recovery from aqueous solutions is more profitable due to its high market value [30,31]. Also there is an increased interest in recovering silver found in trace amounts in copper mines. For the scope of this study Ag^{+} was selected as a representative metal ion. The emphasis was to study effect of silica (non-functionalized) loading on the permeance characteristics of the MMMs, and to demonstrate the applicability of the functionalized silica-MMM technique for silver ion capture (using $AgNO_3$ solution). The MMMs were also characterized, and the separation efficiency was quantified. To the best of our knowledge, it is the first time that thiol-functionalized silica-polymer MMMs have been studied and quantitatively evaluated for silver ion capture. The free surface thiol groups were introduced at the silica surface by silanizing its surface with 3-Mercaptopropyltrimethoxy silane. Ritchie et al., [32] studied polycysteine and other polyamino acid functionalized microfiltration membranes for Hg(II), Pb(II) and Cd(II) capture. Reactive barrier membranes for cesium ion containing silico-titanate as the sacrificial agent were studied by Warta et al., [33]. Some of the studies deal with the application of ion exchange-polymer composite sorbents for heavy metal separations [34-36]. Zhang et al., [37] studied Zr $(HPO_3S)_2$ impregnated cation exchangers for metal ion separations. In the case of pressure driven system studied in this paper, silver ions are transported by convective flow which minimizes diffusional mass transfer limitations. The membrane systems are easier to operate and scale up as compared to the column adsorption techniques.

The specific research goals for this study are:

1. Preparation and characterization of 3-Mercaptopropyltrimethoxy silane functionalized silica particles
2. Preparation and characterization of the MMMs
3. Demonstrate the applicability of the MMMs for silver ion capture and study the effect of various parameters like, silica loading and residence time (by membrane pressure variation) on the capture efficiency
4. Model the transport behavior of silver ion in the membrane matrix

2. Experimental Section

2.1. Materials

Cellulose acetate (M_n = 50,000) and polysulfone (M_n = 16,000; MW = 35,000) were obtained from Aldrich. The solvents used were acetone and dimethyl formamide (DMF) (extra dry, water < 50 mg/L), obtained from Acros Organics. Deionized ultrafiltered water (DIUF) from Fisher Scientific was used for the experiments. The monodispersed Ludox TM-50 particles were obtained from Grace Davison and the silica gels (874-86-2 and 874-85-1) were provided by Huber Corporation. The average particle size, pore diameter and the BET surface area for the three types of silica are given in Table 1. 3-Mercaptopropylthrimethoxy silane (MPTMS) (95%) and 3-(trihydroxysilyl)-1-propane sulfonic acid (35% in water) was obtained from Aldrich. Anhydrous ethanol was obtained from Sigma-Aldrich. Potassium hydrogen phthalate used to calibrate TOC was obtained from Nacalai Tesque Inc. Dextran (482 kDa and 144 kDa) was obtained from Sigma. $AgNO_3$ was obtained from Fisher Scientific and $Ca(NO_3)_2.4H_2O$ was obtained from Mallinckrodt.

2.2. Analysis

The MPTMS functionalized silica was characterized using the Attenuated Total Reflectance – Fourier Transform Infrared (ATR-FTIR) spectroscopy using Varian 7000e FT-IR spectrometer. Total organic Carbon (TOC-5000A) was used to determine concentrations of the dextran solutions. The concentration difference between the feed and permeate was used to calculate dextran rejection. Varian SpectrAA-220 Atomic Absorption Spectrometer (AA) was used to measure concentration difference between the feed and permeate of metal ion solutions (Ag^+ and Ca^{2+}). The wavelengths used for the analysis are 338.3 nm for Ag^+ and 239.9 nm for Ca^{2+}. The analytical error for AA in the case of Ag^+ was approximately 4% for concentrations in the range of 1 to 20 mg/L. All the samples were diluted appropriately in order to use this concentration range. Quartz Crystal Microbalance E4 system from Q-sense was used to study thiol- Ag^+ interaction on 3-mercaptopropyltrimethoxy silane functionalized silica quartz crystal.

2.3. Silica Functionalization

Dry phase deposition method was used to functionalize the silica particles. The particles were dispersed in anhydrous ethanol (15 mL of ethanol per gram of silica) and MPTMS was added such that the ratio of the amount of silica (in g) to the amount of MPTMS (in mL) was 3:7. Ultra high purity grade nitrogen was bubbled through the mixture to evaporate the ethanol under fume hood, thus depositing MPTMS on the surface of the silica. For the silanization reaction, the silica was then placed in oven at 120 °C for 8-10 hrs. The material was allowed to cool and washed twice with 50 mL of anhydrous ethanol to remove any physically adsorbed MPTMS and dried again in oven. The silica was analyzed using FTIR to verify the MPTMS deposition on the silica surface.

2.4. Membrane Preparation

Figure 1 shows a flow chart for the membrane preparation procedure. Two type of membranes were prepared with the polymer backbone of either cellulose acetate or polysulfone. The silica particles were dispersed in the solvent. Polymer was added to this solution and allowed to dissolve. The gel was casted on the glass plate using casting knife. The relative humidity of the room was approximately 45%. Deionized ultra-filtered (DIUF) water bath at 23 °C was used for phase inversion. The membrane casted on the glass plate was immediately immersed into this water bath (no evaporation time).

In the case of cellulose acetate membrane, the solvent was acetone-water mixture in 7.2:1 ratio by volume. The weight of the polymer and the silica was adjusted so as to get the silica loadings of 0, 10, 20 and 30 wt % in the final membranes. In the case of polysulfone, dimethyl formamide was used as a solvent. The silica particles were allowed to disperse in the solvent for minimum of 2 h before adding the polymer to it. Membranes were prepared with final silica loadings of 0, 10, 20, 30 and 40%. Except for 10 wt % silica loading, all other membranes were prepared with the silica type 874-85-1 only. It should be noted that parameters like relative humidity, gelation bath temperature and evaporation time strongly affect the membrane properties and cause variations from batch to batch.

The water permeability of the silica-polymer composite membranes prepared as described above was determined by flux measurements. Sepa ST Membrane Cell from Osmonics was used to carry out the permeance studies. The permeate coming out of the cell was collected at intermittent times to measure the membrane flux (J_W). The membrane flux was measured at various transmembrane pressures and the permeance was obtained as a slope of ΔP vs J_W graph. 100 mg/L solution of dextran (482kDa) was used to study dextran rejection of the polysulfone membranes. Dextran rejection data was used for the estimation of hydrodynamic pore size of the membranes.

2.5. Metal Ion Capture Experiments

Desired concentrations of metal nitrates in deionized ultra filtered water were prepared. The solutions were permeated through the silica mixed matrix membranes using the Osmonics Sepa ST stirred batch membrane cell. Typical area of the membrane used in this cell was approximately 8 cm^2 and the cell volume was 250 ml. After placing the membrane inside the cell, metal ion solution was poured into it (Feed solution). The cell was closed and connected to pressurized nitrogen tank and desired transmembrane pressure (ΔP) was applied by adjusting the regulator to pass the solution through the membrane. The solution was continuously stirred to maintain uniform concentration throughout the cell. The permeate coming out of the cell was collected at intermittent times to measure the metal ion concentration and the membrane flux (J_W). The feed and the permeate were analyzed by atomic absorption spectroscopy. Using the concentrations of the permeate samples and the membrane flux data, the total amount of $AgNO_3$ permeated (mmoles) through the membrane was calculated. Total amount of Ag^+ captured (mmole per g of silica) was calculated by numerical integration over the filtration run.

The effect of the type of metal ion, type of functionalized silica, and residence time was studied on the metal ion capture capacity and the rate of capture. Ag^+ ions are photosensitive and need to be protected from direct light. Hence in all the experiments, the $AgNO_3$ solutions were prepared in amber bottles, and the bottles are covered with aluminum foil.

2.6. Quartz Crystal Microbalance for Metal Ion-Surface −SH interaction

Quartz Crystal microbalance allows the measurement of change in oscillation frequency of a piezoelectric material caused by a change in mass at its surface by adsorption or desorption. Interaction of Ag^+ with surface -SH groups was studied using quartz crystal microbalance. The silica coated quartz crystal (Surface area = 0.785 cm^2) was functionalized with 3-mercaptopropyltrimethoxy silane by deposition from its alcohol based solution. A solution of 95% ethanol and 5% water was prepared and the pH was adjusted to 5 using acetic acid. The pH 5 environment is useful for hydrolysis of methoxy groups of MPTMS and to prevent the disulfide formation of the MPTMS molecules. MPTMS is added with continuous stirring to yield a 2% final concentration. After 10 minutes, allowing the time for hydrolysis and silanol formation, the silica coated quartz crystal was immersed into the solution for 2 minutes. After removing the crystal from solution, it was rinsed free of the excess MPTMS with pure ethanol.

The MPTMS layer was cured for 15 min at 110 °C in oven. This introduced free −SH groups on the crystal surface. The MPTMS functionalized silica crystal was mounted in the QCM cell and pH 5 water was circulated to obtain a steady baseline. It should be noted that only one side of the crystal is in contact with solution throughout the experiment. 100 mg/L Ag^+ solution (pH adjusted to 5 using acetic acid) was passed over the crystal and the interaction of Ag^+ ions with surface −SH was observed in terms of the mass adsorbed at the crystal surface.

3. Results and Discussion

This section discusses the characterization of functionalized silica and silica-polysulfone MMM, the effect of various parameters on metal ion capture behavior, silver-thiol interaction using quartz crystal microbalance, development of model and comparison of experimental and predicted data for silver capture.

3.1. Characterization

The functionalized and the non-functionalized silica were characterized by FTIR. The silica polymer MMM was characterized by SEM imaging. Effect of silica loading on membrane permeability was also studied. Dextran rejection for the membranes was studied to estimate effective pore radius.

Functionalized silica characterization—In order to verify the successful functionalization of the silica (874-85-1) particles with MPTMS, ART-FTIR spectra for the non-functionalized silica and the MPTMS functionalized silica are obtained and compared as shown in Figure 2. The silica material exhibits associated water even after drying. It starts loosing the water only after 250 °C. This causes the non-functionalized silica to exhibit silanol groups (Si-OH) at surface. These groups correspond to the absorbance band around 980 cm^{-1} [38]. The corresponding peak is observed at 960 cm^{-1} in the case of non-functionalized silica. During MPTMS functionalization of the silica surface through the silane chemistry, these free Si-OH groups are consumed. This should cause decrease in the peak intensity for functionalized silica which indeed was observed as represented by diminished peak at 952 cm^{-1}. The strongest peak represents Si-O-Si bond of silica network. In order to roughly quantify the MPTMS surface coverage, the ratio Si-OH: Si-O-Si peak intensities in both the cases are compared. The ratio is 0.054 for non-functionalized silica and 0.011 for functionalized silica. This represents 80% decrease in Si-OH group concentration indicating 80% surface coverage in the case of functionalized silica. This value is in good agreement with maximum coverage of 76% observed [24] for MPTMS monolayer on mesoporous silica.

The adsorption isotherm of the silver with functionalized silica was found to be linear for the conditions in which silver was the limiting factor. In order to characterize the MPTMS functionalized silica, the maximum silver capture capacity was determined by aqueous phase batch experiment. Known amount of silica (g) was added to known volume of Ag^+ solution (pH = 5.8-6.0) of known concentration and the mixture was equilibrated overnight with vigorous shaking. A portion of the mixture was filtered (using 0.22 μm polyvinylidene fluoride membrane) to remove any suspended silica particles and then analyzed for Ag^+ concentration. The difference between the initial concentration and the sample concentration was used to calculate the silver capture capacity for that batch of functionalized silica. The typical silver capture capacity was in the range of 1.5-2.1 mmole of Ag/g of silica. The most of the experiments reported in this study involved silica with a capture capacity of 2.1 mmole/g. If we assume 1:1 stoichiometry between thiol group and silver ion, the silver capture capacity of 2.1 mmole/g leads to 1.8 thiol groups per nm^2 of silica (Based on BET surface area of 708 m^2/g for silica type 874-85-1).

Silica-Polymer MMM characterization—In order to get an idea about the membrane morphology and the silica particle distribution, the MMMs were characterized by SEM imaging. Figure 3 shows the SEM image for a cross-section for 40% Silica-Polysulfone MMM. The cross section clearly displays two regions, a dense top layer followed by a more open structured layer. Silica particles in the dense region are not directly visible, but their impressions can be observed in the image. Some of the Silica particles in the open structure are indicated by the arrows and it can be observed that the silica particles are evenly distributed along the entire membrane thickness. According to the particles size analysis of 874-85-1 silica, performed by Huber Corporation, less than 10% particles are below 2 micron in size and less than 10% particles are greater than 5.1 micron. The average size of the observed particles in the membrane is around 4-5 μm, which is close to their original particle size indicating no additional agglomeration during membrane preparation. This is important towards separation capacity as particle agglomeration may render some sites inaccessible.

Membrane water permeance studies—Effect of silica loading on water permeance of mixed matrix membranes was studied and the results are shown in Figure 4. The error bar corresponds to the standard error of triplicate permeance values measured for membranes prepared from same batch. It was observed that, as the silica loading increased from 10% to 40%, the water permeance of the membranes also increased. Increase in membrane permeance with increasing particle loading was also observed by Zhang et al. [39] in the case of zirconium oxide MMM. The study concluded that increasing particle loading improves pore interconnectivity but does not change skin layer pore size resulting in higher permeance with little effect on retention properties. In our study, membrane water permeance was studied for both functionalized and non-functionalized silica MMMs and there was no significant difference in the two cases. The data can be represented by following linear correlation:

$$A = 1.4 \times 10^{-4} \psi \tag{1}$$

Where A is membrane water permeance in $m^3/(m^2$ s. bar) and ψ is silica weight fraction in membrane (for 10% silica loading $\psi = 0.1$). Equation (1) can be extended to express membrane flux as a function of silica loading as follows:

$$J_w = 1.4 \times 10^{-4} \psi \, \Delta P \tag{2}$$

Where J_W is membrane flux in $m^3/(m^2$ s) and ΔP is applied transmembrane pressure in bar.

Membrane free volume fraction (φ) estimation—Free volume fraction of the membranes was calculated by the membrane water uptake measurements. Silica mixed matrix membrane was soaked in water overnight. The membrane was then removed and lingering water was allowed to drip. The membrane was dabbed lightly with tissue paper to remove any remaining water from the membrane surfaces. The wet membrane was weighed (W_1, kg). The wet membrane was then dried in oven at 110 °C for 8-10 h and the dried membrane was weighed again (W_2, kg). The difference between the weights represents weight of water inside membrane pores. Free volume fraction was calculated using following expression:

$$\varphi = \frac{W_1 - W_2}{A_m L \rho_w} \tag{3}$$

Where, A_m is membrane area (m^2), L is membrane thickness (m) and ρ_W (kg/m^3) is density of water.

Typical value of φ for a MPTMS functionalized 874-85-1 MMM was around 0.6. For the two membranes from same batch the values obtained were 0.58 and 0.63. In order to get an idea about effective pore size of the membrane, dextran rejection was studied. For 10% silica-polysulfone MMM, observed dextran rejection was 51% and 88% using 144kDa and 482 kDa MW dextran, respectively. Hydrodynamic pore radius (r_1) for the membrane was estimated using Ferry-Faxen equation [40,41] which is given below.

$$(1-R)=\left(1-\frac{r_s}{r_1}\right)^2\cdot\left(1-0.104\frac{r_s}{r_1}-5.21\left(\frac{r_s}{r_1}\right)^2+4.19\left(\frac{r_s}{r_1}\right)^3+4.18\left(\frac{r_s}{r_1}\right)^4-3.04\left(\frac{r_s}{r_1}\right)^5\right) \quad (4)$$

R is the rejection of dextran. r_s is the hydraulic radius of the dextran molecule in nm, which can be determined from the following correlation [32]:

$$r_s=0.027\ M^{0.498}$$

M is the molecular weight of dextran in Da.

Based on 482 kDa dextran rejection data (R = 0.88), calculated value for hydrodynamic pore radius was about 39 nm.

Silver capture using silica-polysulfone MMM membrane—Silver capture experiments were carried out to verify Ag^+ removal from its $AgNO_3$ solution using 30% 874-85-1 thiol-functionalized silica MMM. The results are shown in Figure 5. The observed maximum capture was 1.5 mmole Ag/g of silica. The dotted line indicates maximum silver capture capacity. The error bars indicate analytical error of measurement for Ag^+ concentration. In order to prove the hypothesis, that the observed silver capture is specifically due to thiol-Ag^+ interaction, experiments were carried out for silver capture with bare polysulfone membrane and non functionalized silica-polysulfone MMM. It is clearly observed from Figure 5 that silver capture in both the cases is significantly less (0.45 mmole/g of silica) than what was observed for thiol functionalized silica (1.6 mmole/g of silica), hence proving the hypothesis. It should be noted that the non-functionalized silica membrane captured more silver (0.45 mmole/g of silica) than the pure polymer membrane (0.31 mmole/g of silica). Silica is known to have negative charge at the surface and it can attract the positively charged silver ions. This may explain the higher silver capture by non-functionalized silica membrane than the pure polymer membrane.

The concentration of silver on the retentate side was also measured to verify that the difference in feed and permeate concentration is not due to osmotic rejection or Donnan effect. In all the cases, the retentate concentration was less than feed concentration (about 90 – 95% of feed concentration) indicating successful silver capture by the membrane.

In order to understand thiol site accessibility, silver capture experimental results with thiol functionalized silica-MMM in convective mode were compared with soaking mode (no convective flow) results. The membrane was cut into pieces and added to the aqueous silver nitrate solution and the mixture was equilibrated for approximately 12 h. No significant silver capture was observed in the case of soaking mode as opposed to convective mode experiments.

Even if the membrane is highly porous, in the soaking mode the mass transfer resistance for the silver ions to interact with thiol groups inside silica pores is expected to be high. The experimental observation clearly demonstrates the inability of the silver ions to access the thiol sites incorporated inside polysulfone matrix in absence of convective flow.

pH change during silver capture experiments—During silver capture with thiol functionalized silica-MMM, it is hypothesized that the Ag^+ ion replaces hydrogen ion from the −SH (thiol) group and gets adsorbed. This should lead to higher H^+ ion concentration on the permeate side as compared to the feed solution. pH measurement on permeate side indeed showed drop in pH as compared to feed solution. The starting solution pH was 5.8-6.0, and during the initial part of silver pick up experiments (where almost complete silver capture was observed), the observed pH of permeate solution was in the range of 5.3-5.5.

3.2. Effect of Silica surface area and thiol accessibility on metal ion capture

As reported in Table 1, the three types of silica (874-85-1, 874-86-2 and Ludox TM 50) exhibit different particle sizes, pore sizes and correspondingly different specific surface areas. 874-85-1 has higher specific surface area than 874-86-2 and Ludox TM 50. Ludox silica is nonporous as opposed to 874-85-1 and 874-86-2. Hence entire surface area is expected to be accessible for metal ion capture in the case of Ludox. The average pore diameter values (gaps between base particles) are 11.8 nm for 874-86-2 and 3.5 nm for 874-85-1. The smaller pore diameter results in higher specific surface area but it is possible that a portion of this surface area is unavailable for silanization and/or metal ion interaction due to transport limitations.

In order to compare the relative performances of the three types of silica silver capture experiments were carried out with each of the functionalized silica-MMMs under same conditions. The three types of silica were functionalized with MPTMS and then used to make MMMs with cellulose acetate polymer so as to get 10 wt % silica loading in the final membrane. The choice of cellulose acetate over polysulfone for polymer phase was driven by compatibility of the acetone-water-cellulose acetate mixture with Ludox silica which was in the form of aqueous emulsion. The polysulfone-DMF solution did not form homogeneous mixture with Ludox silica. The goal was to select one of the three silica materials based on their relative performance, and then to use that type of silica-polysulfone MMMs for further experiments.

It was hypothesized that the extent of metal ion capture per unit surface area should be largest for Ludox silica. This indeed was observed as shown in Figure 6. It was also observed that 874-86-2 has higher capture capacity per unit surface area than 874-85-1. However, this trend for silver ion capture capacity is reversed when compared in terms of silver ion capture per unit mass of silica present in the membrane as shown in the inset of Figure 6. This clearly indicates that although a fraction of pore surface area of 874-85-1 was not accessible for silver ion capture, the advantage of higher specific surface area outweighs the extent of inaccessibility. 874-85-1 was used as the dispersed phase in the MMMs for all further experiments.

This experiment also established generic applicability of MPTMS functionalized silica MMMs for silver capture using suitable polymer domains (like polysulfone, cellulose acetate etc.). It was also observed that, the silver solution permeance of the cellulose acetate membranes is significantly lower than that of the polysulfone based membranes prepared under similar conditions. For a 10% thiol functionalized cellulose acetate membrane, the permeability was 0.2×10^{-4} cm/s.bar as compared to 1.4×10^{-4} cm/s.bar in the case of polysulfone membranes. This may be attributed to better compatibility of the cellulose acetate-silica leading to formation of tight membrane matrix.

3.3. Effect of Residence time (t_R) on silver capture

High permeate flux at low pressure drop is one of the advantages of membrane applications over conventional packed bed columns. High permeate flux (obtained by applying high transmembrane pressure) leads to lower residence time of the liquid inside membrane, allowing less time for Ag^+ −SH interaction to occur. At the same time high flow rates may increase the throughput of the membrane system. If the Ag^+ −SH interaction is fast (Mass transfer controlled system), higher flow rates should lead to higher rate of silver capture. Experiments were performed at various applied transmembrane pressures (ΔP= 1 to 10 bar) and silver capture was studied. The results are shown in Figure 7.

The residence times were calculated by dividing the water uptake of the membrane (W_1-W_2) by experimental flow rates observed during the silver capture. The dotted line represents maximum silver capture capacity of the functionalized silica (2.1 mmole of Ag^+/g of silica). The solid straight line indicates the ideal case where all the silver permeated through the membrane is captured. In the initial part of the experiment all the silver was captured in all the cases indicated by the data points lying on top of the solid line. As the amount of silver permeated increased further, deviations from the ideal case were observed. In the case of lower residence times t_R = 6.5 s and t_R = 2.8 s), a plateau behavior is observed at approximately 80% capture capacity.

The inset represents the same data plotted in the form of amount of silver captured with respect to time. It is clearly observed that the rate of silver capture increases with increasing permeate flux within the experimental conditions studied. This indicates that under the experimental flow conditions, the Ag^+-SH interaction is mass transport limited. Due to this mass transport limited interaction, available thiol sites are consumed faster owing to higher quantity of silver fed per unit time in the case of t_R = 2.8 s.

If the sites are getting exhausted faster, after a point higher amount of silver ions (in the form of $AgNO_3$) will start coming out on the permeate side. This will lead to increased deviations from the ideal case. As expected, the deviations are highest for lowest residence time as observed in Figure 7. The maximum silver capture observed for t_R = 20 s even exceeded the maximum silver capture capacity of the silica. It is possible that while determining maximum capacity, some of the silica particles agglomerate in the process and a fraction of −SH sites become inaccessible. In the case of MMM there may be reduced agglomeration as the particles are trapped inside membrane polymer matrix resulting in better accessibility.

Dynamic capacity—In order to compare the relative performance of the membranes towards removal of silver ion applications, dynamic capacity was calculated in each case. The dynamic capacity was defined as amount of silver captured which was calculated by numerical integration over the filtration run until the point where the permeate concentration was approximately 10% of feed concentration. The capacity was normalized by dividing with maximum silver capture capacity (2.1 mmole/g) and results are shown in Figure 8. It can be observed that dynamic binding capacity initially decreases with increasing membrane flux from 70% to 45%, but remains almost constant thereafter. Figure 8 implies that the dynamic capacity is constant for J_W higher than 3×10^{-5} m/s. The constant binding capacity in the high flux regime indicates there is sufficient time for Ag^+ −SH interaction and the process is mass transfer controlled.

Selectivity of Ag^+/Ca^{2+} Capture—In order to verify the selectivity of the MMMs towards Ag^+ ion, silver capture was studied from a feed containing equimolar concentration of Ag^+ and Ca^{2+} (Metal nitrates used to prepare corresponding solutions). The results are shown in Figure 9. It can be clearly observed that the membrane selectively captured Ag^+ from the metal ion mixture. The Ca^{2+} capture was negligible. Owing to the nature of the silver-thiol interaction

it is expected that even in very high concentration of other metal ions like Na^+ and Ca^{2+}, the selectivity towards silver will be high. This characteristic is important for selective capture of heavy metal ions from a metal ion mixture which usually is the case in many practical applications. Ritchie et al., [32] have studied selectivity of similar membrane adsorbent systems towards target metal in very high excess of other metal ions and found that approximately 70% of the target metal is captured in the single pass.

Membrane Regeneration and Reuse—Several studies have been reported in the literature dealing with regeneration of thiol based sorbents and recovery of silver/mercury metals. The most common technique used is sorbent treatment with highly acidic solution like 12 M HCl [24,42]. These harsh conditions can affect the sorbents and significant decrease in sorption capacity is observed in some cases.

In this study, experiments were conducted to test the membranes for silver recovery. Even after passing pH 2 aqueous solutions through the membranes, no silver recovery was observed. Highly acidic solutions (pH < 2) were thought to be detrimental to the MMMs prepared in this study. Another experiment was performed with silica functionalized with thiol as well as sulfonic acid groups. The silica was prepared in the similar manner as described earlier using the combination of MPTMS and 3-(trihydtoxysilyl)-1-propane-sulfonic acid. For the solution phase experiment 25% of the silver captured was removed from silica surface by lowering the pH of the solution to 1.8. More experiments to check the regeneration reuse and selectivity of such silica material towards silver capture will be required to optimize the conditions.

Hudson et al., [43] employed acidic potassium cyanide solution (2M HNO_3) and reported 100% regeneration and reuse of thiol based polymeric resin for silver capture.

Another approach applied for regeneration and recovery is to use mildly acidic (0.1 N HCl) thiourea solution as an eluent [29,42]. Thiourea acts as a complexing legend in the eluent. 80-90% metal recovery with retained sorption capacity was obtained.

In our case, it seems that acidic thiourea treatment may be useful for regeneration. Strongly acidic conditions can damage the functionalized silica and result into loss of sorption capacity. However, due to the high market value of silver, scarifying the sorbent for silver recovery may still be economically viable.

3.4. Quartz Crystal Microbalance to study surface SH- Ag^+ interaction

In order to understand the Ag^+ -SH interaction and to establish the thiol group density (number of thiol groups per nm^2 of silica surface), quartz crystal microbalance was utilized. This can also be used to establish sorption kinetics as the extent of sorption can be measured in nano-gram range. Figure 10 shows the adsorption data for the QCM experiment. The arrows indicate the time at which the feed solution is changed from water to silver solution or vice a versa. The adsorbed mass increased until 300×10^{-4} mmole/m^2 and reached equilibrium. The discontinuity in the increasing adsorbed mass at 230×10^{-4} mmole/m^2 represents water passage to check if the adsorbing mass is non-specifically adsorbed. At 300×10^{-4} mmole/m^2, passage of water caused some desorption and the adsorbed mass steadied at 250×10^{-4} mmole/m^2. On further passage of Ag^+ solution, adsorbed mass increased to 320×10^{-4} mmole/m^2 and stayed at that value even after repeated passing of water and Ag^+ solution alternatively. A similar experiment with non-functionalized silica crystal showed some adsorption on passage of Ag^+ solution which desorbed completely on passage of water indicating no specific Ag^+ adsorption.

In order to convert the adsorbed mass in moles of Ag^+ adsorbed, it was assumed that the hydrogen ion of −SH group was exchanged with the Ag^+. This means that 1 mole of Ag^+

adsorption causes 106 g increase in the adsorbed mass. The calculated equilibrium adsorbed value of 320×10^{-4} mmole of silver/m^2 corresponds to 19×10^{18} thiol groups per square meter. For fully dense monolayer coverage of MPTMS on silica, Feng et al. [24] have reported a value of 5×10^{18} molecules per square meter. The higher surface density of thiol groups may be attributed to multilayer MPTMS coverage or adsorbed mass overestimation by QCM [44-46] due to coupled water of hydration with Ag^+.

3.5. Concentration Profile of Ag^+ in functionalized silica mixed matrix membrane

The silver capture by functionalized silica MMMs was modeled to predict concentration profile of silver ion along the membrane thickness at varying time. Due to the spongy morphology of the silica MMM, a membrane pore based model was deemed unsuitable in this case. The membrane pore based model incorporates core flow. In the case of adsorptive separation process like this, core flow leads to immediate appearance of the adsorbate on the permeate side. The observation of the experimental break-through curves clearly indicate that the capture efficiency is almost 100% for a substantial time in all the cases demonstrating absence of core flow. It was thought suitable to model this MMM process as a one dimensional unsteady state problem. The MMM can be described in terms of three different phases i.e. active silica adsorbent phase, inert polymer phase and aqueous silver solution phase occupying the free volume fraction of the membrane. Figure 11 shows schematics of a MMM as a combination of the three phases. For the modeling purpose, the silica particles are assumed to be impermeable and non-porous. It should be noted that, throughout the model calculations, SI units were used for all the quantities but in the Figures the quantities were converted to suitable units in order to aid comparison and discussion of the experimental and predicted results. Following terminology was used for modeling purpose:

φ = Free volume fraction; φ_p = Polymer volume fraction; $(1-\varphi-\varphi_p)$ = Fractional volume of silica particles; C' = Concentration of Ag^+ in bulk liquid phase (moles of Ag^+/m^3 of Liquid); q' = Concentration of silver in silica phase (moles of Ag^+/m^3 of silica Particles); q_{eq} = maximum concentration of silver in silica phase for C' (moles of Ag^+/m^3 of silica Particles); J_W = Membrane Flux (m/s); t' = time (s); z' = Distance down the membrane thickness (m).

Taking a mass balance on the liquid phase over an element shown in Figure 11 we get,

$$\varphi\frac{\partial C\prime}{\partial t\prime}+J_w\frac{\partial C\prime}{\partial z\prime}+(1-\varphi-\varphi_p)\frac{\partial q\prime}{\partial t\prime}=0 \tag{A}$$

Similarly, taking a mass balance on the solid silica phase we get,

$$\frac{\partial q\prime}{\partial t\prime}=k(q_{eq}-q\prime) \tag{B}$$

With initial conditions as follows:

$$C\prime(0,t\prime)=C_0$$
$$q\prime(z,0)=0$$
$$C\prime(z\prime,0)=0$$

In this case, the axial diffusion is neglected as compared to axial convection.

In order to couple equations (A) and (B), following linear relationship between q_{eq} and C' was assumed.

$$q_{eq}=\gamma C' \tag{C}$$

Where

γ = Silver − thiol affinity constant.

In this case γ will be a function of surface density of thiol groups. Substituting from equation (C) into equation (B) we get,

$$\frac{\partial q'}{\partial t'}=k(\gamma C' - q') \tag{D}$$

The equations can be made dimensionless by defining following variable

$$C=\frac{C'}{C_0};q=\frac{q'}{q_\infty};z=\frac{z'}{L} \text{ and } t=\frac{t'}{T_s}$$

Where,

C_0 = Inlet feed concentration of silver ion (mole/m3); q_∞ = maximum silver capture (moles of Ag/m^3 of silica); L = Membrane thickness (m). T_S = Time at which saturation of silver capture was observed and experiment was terminated (s). The saturation time varied between 60 min to 400 min for various cases studied.

The dimensionless system of PDEs is

$$\frac{\varphi L}{J_w T_s}\frac{\partial C}{\partial t}+\frac{\partial C}{\partial z}+(1-\varphi-\varphi_p)\frac{kL}{J_w}(\gamma C - q\frac{q_\infty}{C_0})=0 \tag{A1}$$

$$\frac{\partial q}{\partial t}=\frac{kT_s C_0}{q_\infty}(\gamma C - q\frac{q_\infty}{C_0}) \tag{B1}$$

With corresponding initial conditions

$$C(0,t)=1$$
$$q(z,0)=0$$
$$C(z,0)=0$$

Femlab™ (COMSOL, version 3.0a) was used to solve the set of two unsteady state partial differential equations (A1 and B1). Multiphysics convection-diffusion transient state analysis

was applied to the one dimensional domain. The thickness of the membrane was partitioned into 120 elements (241 nodes). In order to get a stable solution it was required to add artificial diffusion term in the case of equation (A1). In the absence of artificial diffusion term an unstable oscillating numerical solution is obtained. In the later part, it will also be demonstrated that addition of this term does not affect the solution of the system. In order to do this, option of compensated Petrov-Galerkin method was selected in this particular case.

The required values of the model parameters are obtained from the experimental conditions and are as follows:

C_0 = Feed Ag^+ concentration = 1.03 mole/m^3 (112 mg/L)

$L = 150 \times 10^{-6}$ m (Membrane thickness measured experimentally)

$\varphi = 0.63$ (Obtained from membrane water uptake experiment)

Volume fraction of polymer in MMM can be calculated by following expression

$$\varphi_p = \frac{\rho_{Si}(1-\varphi)(1-\psi)}{\rho_{Si}(1-\psi)+\psi\rho_p} \tag{5}$$

Where, ρ_{Si} is density of silica (2.2 g/cm^3) and ρ_p is density of polysulfone (1.24 g/cm^3) For a 40% Silica-Polysulfone MMM ($\psi = 0.4$), using equation (5), $\varphi_p = 0.27$

From silver capture experiment with functionalized silica particles only, maximum extent of silver capture was 2.1×10^{-3} mole/g of silica (4.62×10^3 mole of Ag/m^3 of silica), for feed concentration of 100 mg/L (0.92 mole/m^3).

Using this data calculated value for $\gamma = 5021.8$

By applying varying transmembrane pressure, the residence time (t_R) was varied. The corresponding membrane flux (J_W, m/s) in the three cases studied are 9.4×10^{-6} (t_R = 20 s), 3×10^{-5} (t_R = 6.5 s), and 6.93×10^{-5} (t_R = 2.8 s).

In order to apply artificial diffusion to get a stable numerical solution, a value for silver diffusivity in the aqueous phase was required. Based on the reported data [47], a calculated $AgNO_3$ diffusivity value of 1.80×10^{-9} m^2/s was used for all the calculations. The only unknown parameter remaining was the volumetric mass transfer coefficient (k). In the case of $J_W = 6.93 \times 10^{-5}$ m/s, k was used as an adjustable parameter to match the predicted data with experimental data. The comparison of the experimental and predicted breakthrough curves is shown in Figure 12. The predicted data matches very well with the experimental data until C = 0.80. Deviations are higher beyond this point. The fitted value of the mass transfer coefficient is 0.0045 s^{-1}. The value of mass transfer coefficient for packed colums (Gas-Liquid) is generally in the range of 0.005-0.02 s^{-1} [48]. In order to quantify model quality, R^2 value based on Predicted Error Sum of Squares (PRESS statistics) was calculated using following expression:

$$R^2 = 1 - \frac{\sum_{i=1}^{n}[y_i - \widehat{y_i}]^2}{\sum_{i=1}^{n} y_i^2 - n\bar{y}_i^2} \tag{6}$$

Where, y_i is experimental value, $\hat{y_i}$ is predicted value, $\bar{y_i}$ is mean of experimental values and n is number of data points used for calculation.

In this case the R^2 value for the fit is 0.92 indicating a good fit. The sensitivity of the model towards diffusivity is determined by varying it from 1×10^{-10} to 1×10^{-8} m^2/s and it was observed that the predicted outlet concentration changes by less than 1% over this range. This also indicates that the artificial diffusion term does not have any significant effect on the solution of the system. This also supports the assumption that diffusion is negligible as compared to convection in this case. The model sensitivity was also determined for 10% error in γ value (5021.8). Using $\gamma = 4519.6$ (case I) and $\gamma = 5524.0$ (case II), the corresponding values of mass transfer coefficients were obtained so as to fit the predicted data to the experimental data. The adjusted values are $k = 0.0055$ s^{-1} ($R^2 = 0.89$) and $k = 0.0038$ s^{-1} ($R^2 = 0.93$) for case I and case II, respectively.

It is expected that the value of k will vary with the permeation rate. In order to predict the breakthrough curve data for varying membrane fluxes without any adjustable parameter, a correlation between mass transfer coefficient and membrane flux was required. Based on various mass transfer correlations reported in literature, it was thought that $k \alpha J_w^{0.5}$ is a reasonable assumption. Using the value of $k = 0.0045$ s^{-1} for corresponding $J_W = 6.93 \times 10^{-5}$ m/s, the value of the proportionality constant is estimated to be 0.541. This leads to following mass transfer correlation:

$$k = 0.541\, J_w^{0.5} \tag{7}$$

Expression (7) was used to calculate the volumetric mass transfer coefficients for varying membrane fluxes. These values of k were used to predict the breakthrough curve data and the comparisons of the predicted data with the experimental data are shown in figure 13. Inset shows the comparison in the case of silver capture with 30% silica loading-MMM at $J_W = 8.5 \times 10^{-6}$ m/s ($R^2 = 0.91$). In all the cases the onset of breakthrough is predicted accurately but deviations are observed when the capture process approaches saturation. The deviations are highest in the case of $J_W = 9.4 \times 10^{-6}$ m/s ($R^2 = 0.75$). Considering the fact that no adjustable parameter was used, the model predictions are comparable with experimental observations. As discussed earlier, the assumption of negligible diffusion compared to convection has been verified for $J_W = 6.93 \times 10^{-5}$ m/s. It is expected that the role of diffusivity will be of greater importance for the lowest membrane flux and hence model sensitivity towards diffusivity was also determined for $J_W = 9.4 \times 10^{-6}$ m/s. It was observed that, by varying diffusivity values between 1×10^{-10} to 1×10^{-8} m^2/s, the predicted outlet concentration changes by less than 1%.

In order to check the model applicability over a wide range of parameters, model was used to predict results for silver capture experiment using a stack of two membranes. Multi stack membranes are often used to increase capacity of existing membrane processes. MPTMS functionalized 874-85-1 40% Silica-polysulfone MMM membranes were stacked together and silver solution was permeated through the stack. The silica used was deliberately functionalized under the conditions where MPTMS was the limiting reactant so as to get reduced silver capture capacity per gram of silica. The corresponding parameters obtained from experimental characterization of silica and MMM are as follows: Membrane thickness = 1.1×10^{-4} m for one membrane i.e. $L = 2.2 \times 10^{-4}$ m for the stack; $\varphi = 0.52$; $\varphi_p = 0.35$; $\gamma = 1880.3$ (as compared to 5021.8 in previous cases). Concentration of feed solution $C_0 = 0.874$ mole/m^3. Using these parameters, predicted breakthrough curve was obtained (dotted line) and its comparison with experimental results is shown in Figure 14. The R^2 value based on PRESS statistics for this fit is 0.85. It can be observed that the model consistently overestimated exit silver ion

concentration throughout this run but follows the overall trend in the data. The deviations are partially attributed to the inaccurate value of mass transfer coefficient obtained from the correlation based on single stack data.

The reasonable agreement between experimental and predicted data in above demonstrated cases proves that the model is helpful to predict experimental results over a wide range of operating conditions and parameters like silica loading, membrane flux, silver capture capacity of silica, and membrane thickness.

Prediction of silver concentration in silica phase—The model also provides information about concentration of silver in silica phase throughout the membrane as a function of time. Figure 15 displays predicted silver concentration (mmole of Ag captured/g of silica) profile along the membrane thickness at varying experimental time for $J_W = 6.93 \times 10^{-5}$ m/s. As expected, the silver concentration is highest near feed side and gradually decreases along the membrane thickness. It can be also observed that the membrane is almost fully saturated with Ag in 60 minutes.

Silver concentration profile along the membrane thickness—It is also possible to predict concentration profile of silver ion at desired positions along the membrane thickness using the model. It is expected that the near the position from the membrane feed side, the earlier it will saturate. This indeed was observed as shown in Figure 16. The results represents silver capture using 40% silica loading silica-polysulfone membrane ($\varphi = 0.63$; $\varphi_p = 0.27$ and $J_W = 6.93 \times 10^{-5}$ m/s). A predicted result for a two stack membrane (z = 1) is also shown for comparison with single stack membrane. The model offers an efficient way to study effect of various experimental parameters on silver or other metal separation. The model is applicable for a generic case involving MMM for liquid phase applications.

Conclusions—Thiol functionalized silica-polysulfone MMMs were successfully applied for silver ion separation from aqueous solutions. The effects of various parameters like residence time, porous/nonporous nature, and specific surface area of the silica materials on the silver capture efficiency were studied. The silver capture data at varying residence times implied that the dynamic silver capture capacity initially decreases with increasing membrane flux and then become constant for higher fluxes. Ludox silica, being nonporous, offers highest accessibility towards thiol-silver interaction. However 874-85-1 type silica demonstrated highest silver capture capacity (approximately 2mmole of silver per g of silica) among the three silica materials studied. It was observed that the silver-thiol interaction in the MMMs is mass transfer controlled under the experimental conditions. The specific nature of the thiol-silver interaction allows selective silver capture from aqueous solution containing other metal ions like calcium and copper. This property is important towards practical application of the MMMs, as the feed stream often contains other metal ions in high concentrations. The silver capture data was successfully predicted without any adjustable parameter using a one dimensional unsteady state model. The reasonable agreement between experimental data and predicted data demonstrates applicability of the model over a broad range of operating parameters like membrane flux, silica loading, silver capture capacity of the functionalized silica material, and membrane thickness. The concept of MMMs can be easily expended to the capture of other heavy metal like mercury, lead etc. The MMMs provide a very good platform for application of thiol functionalized silica materials for silver ion separations.

Acknowledgments

The authors acknowledge the support of Huber Corporation for this research. P. Fraile was a NSF/REU student. Partial support was also provided by the NIEHS-SBRP program.

References

1. Chung TS, Jiang LY, Li Y, Kulprathipanja S. Mixed matrix membranes (MMMs) comprising organic polymers with dispersed inorganic fillers for gas separation. Progress in Polymer Science 2007;32:483–507.
2. Nunes, SP.; Peinemann, KV. Membrane Technology: In the chemical industry. Wiley-VCH; Singapore: 1987.
3. Kulprathipanja, S.; Neuzil, RW.; Li, NN. Gas separation by means of mixed matrix membranes. Allied-Signal, Inc.; USA: 1988. p. 7Application: US USCont of U S Ser No 697,990, abandoned
4. Mahajan R, Koros WJ. Factors Controlling Successful Formation of Mixed-Matrix Gas Separation Materials. Industrial & Engineering Chemistry Research 2000;39:2692–2696.
5. Mahajan R, Koros WJ. Mixed matrix membrane materials with glassy polymers. Part 1. Polymer Engineering and Science 2002;42:1420–1431.
6. Mahajan R, Koros WJ. Mixed matrix membrane materials with glassy polymers. Part 2. Polymer Engineering and Science 2002;42:1432–1441.
7. Robeson LM. Correlation of separation factor versus permeability for polymeric membranes. Journal of Membrane Science 1991;62:165–85.
8. Lape NK, Yang C, Cussler EL. Flake-filled reactive membranes. Journal of Membrane Science 2002;209:271–282.
9. Liu Q, Cussler EL. Barrier membranes made with lithographically printed flakes. Journal of Membrane Science 2006;285:56–67.
10. Shimotori T, Cussler EL, Arnold WA. Diffusion of mobile products in reactive barrier membranes. Journal of Membrane Science 2007;291:111–119.
11. Okumus E, Gurkan T, Yilmaz L. Development of a mixed-matrix membrane for pervaporation. Separation Science and Technology 1994;29:2451–73.
12. Adoor SG, Sairam M, Manjeshwar LS, Raju KVSN, Aminabhavi TM. Sodium montmorillonite clay loaded novel mixed matrix membranes of poly(vinyl alcohol) for pervaporation dehydration of aqueous mixtures of isopropanol and 1,4-dioxane. Journal of Membrane Science 2006;285:182–195.
13. Vane LM, Namboodiri VV, Bowen TC. Hydrophobic zeolite-silicone rubber mixed matrix membranes for ethanol-water separation: Effect of zeolite and silicone component selection on pervaporation performance. Journal of Membrane Science 2008;308:230–241.
14. Lin YF, Ma CCM, Lin YY, Yen CY, Hung CH. High proton-conducting sulfonated poly(ether ether ketone)/functionalized mesoporous silica composite membranes. Key Engineering Materials 2007:334–335. 945–948.
15. Sambandam S, Ramani V. SPEEK/functionalized silica composite membranes for polymer electrolyte fuel cells. Journal of Power Sources 2007;170:259–267.
16. Yen CY, Lee CH, Lin YF, Lin HL, Hsiao YH, Liao SH, Chuang CY, Ma CCM. Sol-gel derived sulfonated-silica/Nafion composite membrane for direct methanol fuel cell. Journal of Power Sources 2007;173:36–44.
17. Avramescu ME, Girones M, Borneman Z, Wessling M. Preparation of mixed matrix adsorber membranes for protein recovery. Journal of Membrane Science 2003;218:219–233.
18. Saiful, Borneman Z, Wessling M. Enzyme capturing and concentration with mixed matrix membrane adsorbers. Journal of Membrane Science 2006;280:406–417.
19. Makkuni A, Varma RS, Sikdar SK, Bhattacharyya D. Vapor Phase Mercury Sorption by Organic Sulfide Modified Bimetallic Iron-Copper Nanoparticle Aggregates. Industrial & Engineering Chemistry Research 2007;46:1305–1315.
20. Zhang L, Zhang W, Shi J, Hua Z, Li Y, Yan J. A new thioether functionalized organic-inorganic mesoporous composite as a highly selective and capacious Hg2+ adsorbent. Chemical Communications (Cambridge, United Kingdom) 2003:210–211.
21. Kang T, Park Y, Yi J. Highly selective adsorption of Pt2+ and Pd2+ using thiol-functionalized mesoporous silica. Industrial & Engineering Chemistry Research 2004;43:1478–1484.
22. Vieira EFS, De J, Simoni A, Airoldi C. Interaction of cations with SH-modified silica gel: thermochemical study through calorimetric titration and direct extent of reaction determination. Journal of Materials Chemistry 1997;7:2249–2252.

23. Nakamura T, Yamada Y, Yano K. Direct synthesis of monodispersed thiol-functionalized nanoporous silica spheres and their application to a colloidal crystal embedded with gold nanoparticles. Journal of Materials Chemistry 2007;17:3726–3732.
24. Feng X, Fryxell GE, Wang LQ, Kim AY, Liu J, Kemner KM. Functionalized monolayers on ordered mesoporous supports. Science (Washington, D.C.) 1997;276:923–926.
25. Liu C, Huang Y, Naismith N, Economy J, Talbott J. Novel Polymeric Chelating Fibers for Selective Removal of Mercury and Cesium from Water. Environmental Science and Technology 2003;37:4261–4268. [PubMed: 14524462]
26. Park JH, Kim YG, Oh C, Shin SI, Kim YC, Oh SG, Kong SH. Fabrication of hollow silver spheres by MPTMS-functionalized hollow silica spheres as templates. Materials Research Bulletin 2005;40:271–280.
27. Vieira EFS, Cestari AR, Simoni JdA, Airoldi C. Use of calorimetric titration to determine thermochemical data for interaction of cations with mercapto-modified silica gel. Thermochimica Acta 1999;328:247–252.
28. Pearson RG. Hard and soft acids and bases, HSAB, part 1: Fundamental principles. Journal of Chemical Education 1968;45:581–587.
29. Atia AA, Donia AM, Yousif AM. Comparitive study of the recovery of silver(I) from aqueous solutions with different chelating resins derived from glycidyl methacrylate. Journal of Applied Polymer Science 2005;97:806–812.
30. Abasalan G, Mehrdjardi MA. Separation and preconcentration of silver ion using 2-mercaptobenzothiazole immobilized on surfactant-coated alumina. Separation and Purification Technology 2003;33(1):95–101.
31. Trochimczuk AW, Kolarz BN. Synthesis and chelating properties of resins with methylthiourea, guanylthiourea and dithiocarbamate groups. European Polymer Journal 2000;36(11):2359–2363.
32. Ritchie SM, Kissick KE, Bachas LG, Sikdar SK, Parikh C, Bhattacharyya D. Polycysteine and Other Polyamino Acid Functionalized Microfiltration Membranes for Heavy Metal Capture. Environmental Science and Technology 2001;35(15):3252–3258. [PubMed: 11506016]
33. Warta AM, Arnold WA, Cussler EL. Permeable Membranes Containing Crystalline Silicotitanate As Model Barriers for Cesium Ion. Environmental Science and Technology 2005;39(24):9738–9743. [PubMed: 16475361]
34. Khan AA, Alam MM. New and novel organic-inorganic type crystalline ‘polypyrrole/polyantimonic acid’ composite system: preparation, characterization and analytical applications as a cation-exchange material and Hg(II) ion-selective membrane electrode. Analytica Chimica Acta 2004;504:253–264.
35. Hernandez MEP, Arteaga KA, Vidal CAG, Pardave MP, Romo MR, Silva MTR. Mercury ions removal from aqueous solution using an activated composite membrane. Environmental Science and Technology 2005;39:7667–7670. [PubMed: 16245842]
36. Pan BC, Zhang QR, Zhang WM, Pan BJ, Du W, Lv L, Zhang QJ, Xu ZW, Zhang QX. Highly effective removal of heavy metals by polymer -based zirconium phosphate: A case study of lead ion. Journal of Colloid and Interface Science 2007;310(1):99–105. [PubMed: 17336317]
37. Zhang Q, Pan B, Pan B, Zhang W, Jia K, Zhang Q. Selective Sorption of Lead, Cadmium and Zinc Ions by a Polymeric Cation Exchanger Containing Nano-Zr(HPO3S)2. Environmental Science & Technology 2008;42(11):4140–4145. [PubMed: 18589978]
38. Boccuzzi F, Coluccia S, Ghiotti G, Morterra C, Zecchina A. Infrared study of surface modes on silica. Journal of Physical Chemistry 1978;82:1298–303.
39. Zhang Y, Li H, Lin J, Li R, Liang X. Preparation and characterization of zirconium oxide particles filled acrylonitrile-methyl acrylate-sodium sulfonate acrylate copolymer hybrid membranes. Desalination 2006;192:198–206.
40. Ferry JD. Statistical evaluation of sieve constants in ultrafiltration. Journal of General Physiology 1936;20:95–104. [PubMed: 19872986]
41. Lindau J, Jonsson AS, Bottino A. Flux reduction of ultrafiltration membranes with different cut-off due to adsorption of a low-molecular-weight hydrophobic solute-correlation between flux decline and pore size. Journal of Membrane Science 1998;149:11–20.

42. Walcarius A, Delacote C. Mercury(II) binding to thiol-functionalized mesoporous silicas: critical effect of pH and sorbent properties on capacity and selectivity. Analytica Chimica Acta 2005;547 (1):3–13.

43. Hudson MJ, Shepherd MJ. Selective extraction and separation of metals especially silver (and copper) using poly(2-S-vinyl-1,3,4-thiadiazole-5-thiol). Hydrometallurgy 1983;9(3):223–34.

44. Caruso F, Serizawa T, Furlong DN, Okahata Y. Quartz Crystal Microbalance and Surface Plasmon Resonance Study of Surfactant Adsorption onto Gold and Chromium Oxide Surfaces. Langmuir 1995;11:1546–52.

45. Rinia HA, Caruso F, Furlong DN. Gravimetric Monitoring of Nonionic Surfactant Adsorption from Nonaqueous Media onto Quartz Crystal Microbalance Electrodes and Colloidal Silica. Langmuir 1996;12:2145–52.

46. Stalgren JJR, Eriksson J, Boschkova K. A Comparative Study of Surfactant Adsorption on Model Surfaces Using the Quartz Crystal Microbalance and the Ellipsometer. Journal of Colloid and Interface Science 2002;253:190–195. [PubMed: 16290846]

47. Cussler, EL., editor. Diffusion: Mass transfer in fluid systems. Second. 1996.

48. Perry, RH.; Green, DW., editors. Perry's Chemical Engineers' Handbook. Seventh. 1997. p. 23-44.

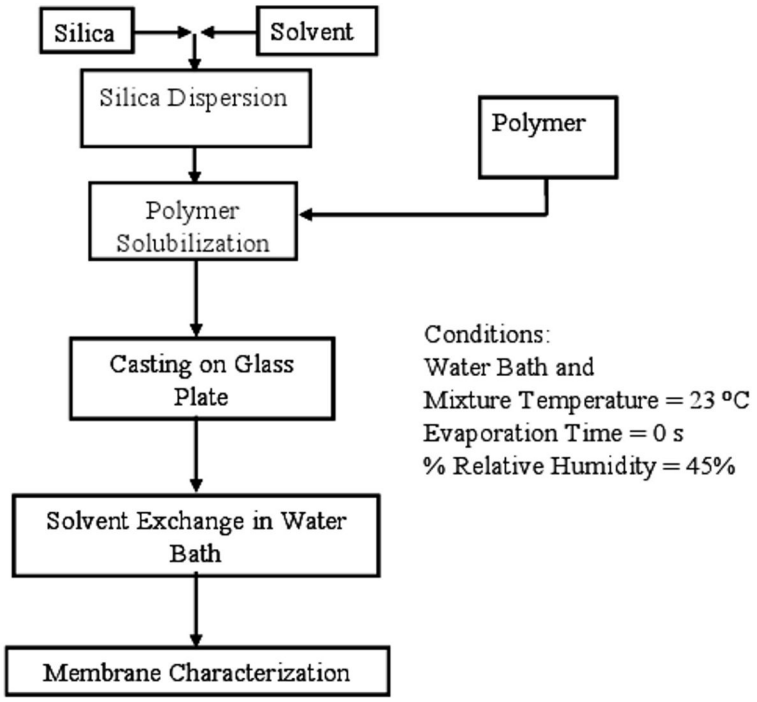

Figure 1. Flow diagram for membrane preparation procedure

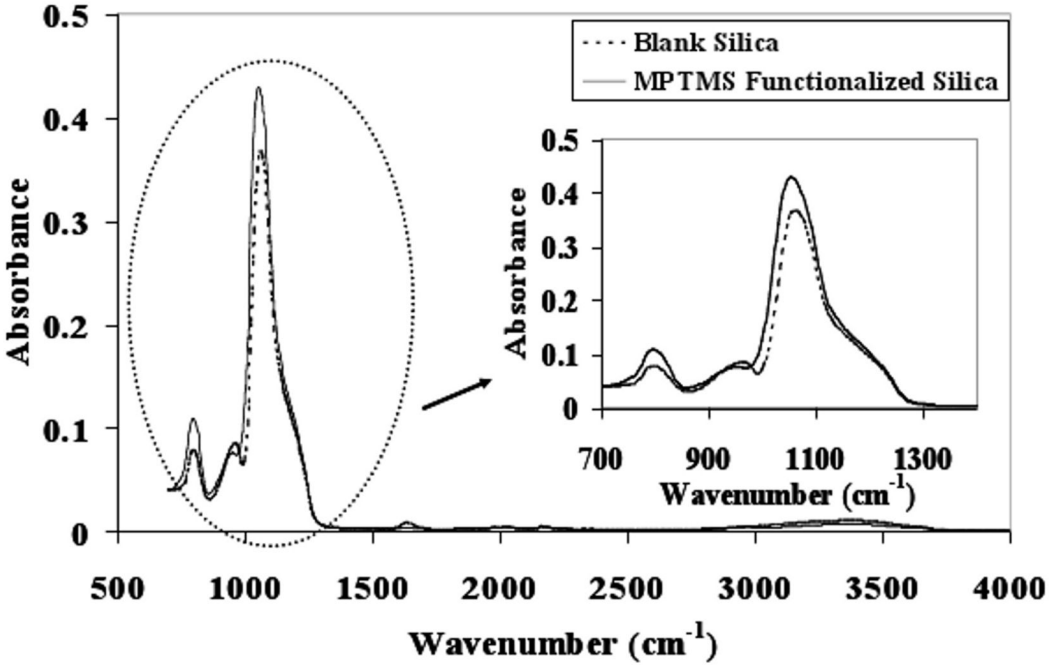

Figure 2. FTIR-ATR for blank and MPTMS functionalized silica (874-85-1). The peak representing free Si-OH groups on silica surface (959 cm-1) diminishes in the case of MPTMS functionalized silica

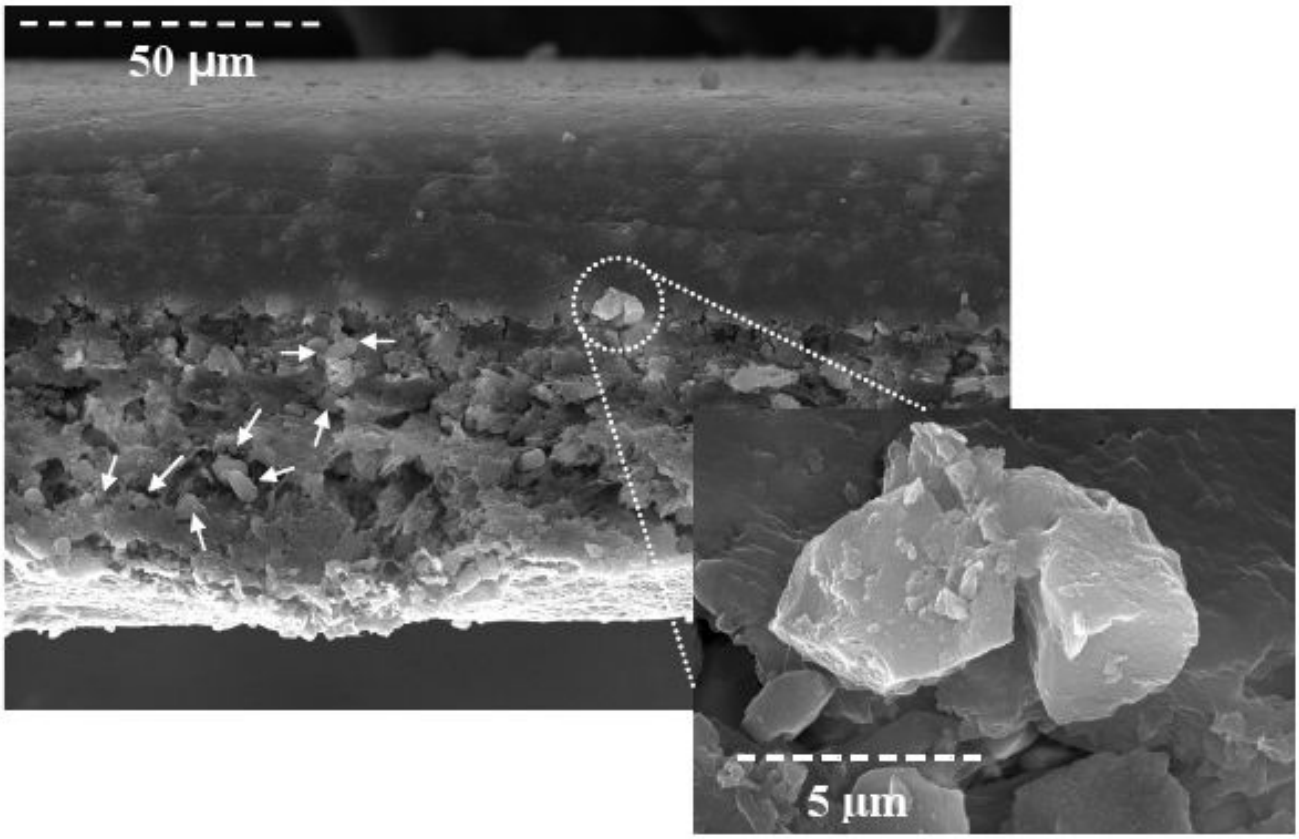

Figure 3. SEM image of cross-section of 874-85-1 MPTMS functionalized 40% silica-polysulfone MMM. Arrows point to some of the silica particles in membrane matrix indicating their uniform distribution along the membrane thickness

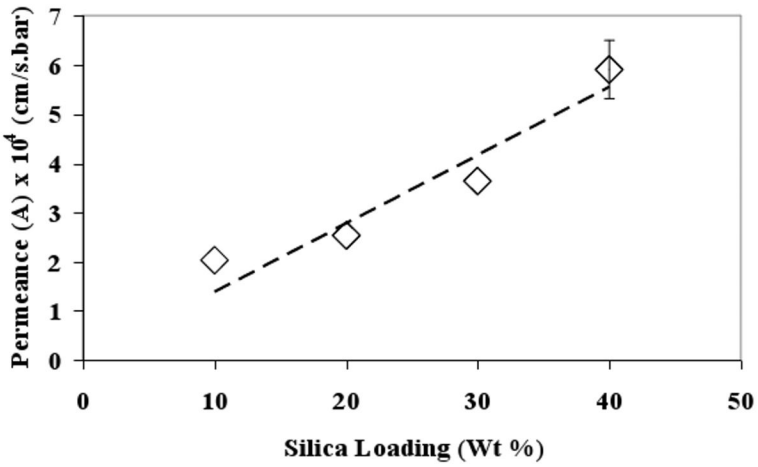

Figure 4. Effect of silica loading on membrane water permeance for non-functionalized 874-85-1 silica-polysulfone mixed matrix membrane. Dotted line indicates fitted linear correlation for the data (R^2 = 0.91)

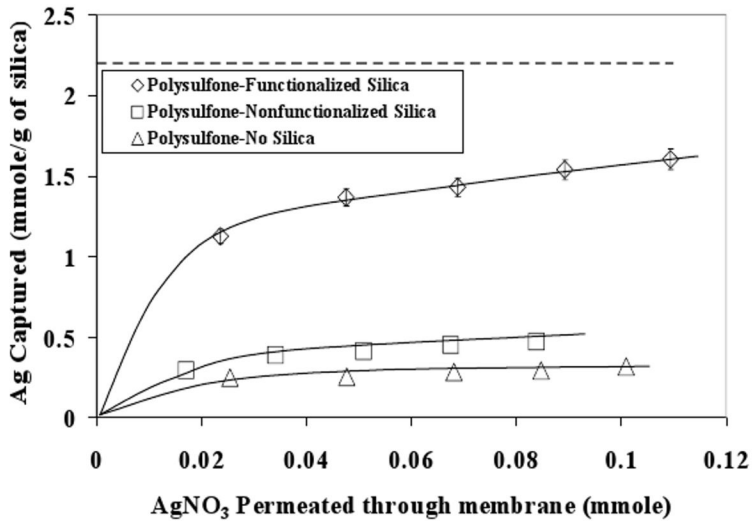

Figure 5. Silver capture using thiol-functionalized 30 % 874-85-1 silica-polysulfone MMM. Comparison with non-functionalized silica-MMM and bare polysulfone membrane silver capture. Dotted line indicates maximum silver capture capacity. Error bars indicate analytical error of measurement for Ag^+ concentration. In order to facilitate comparison, the values reported for the case of bare polysulfone membrane (mmole/g of silica), are based on amount of silica present in polusulfone-non functionalized silica case. The solid lines show trends in the data

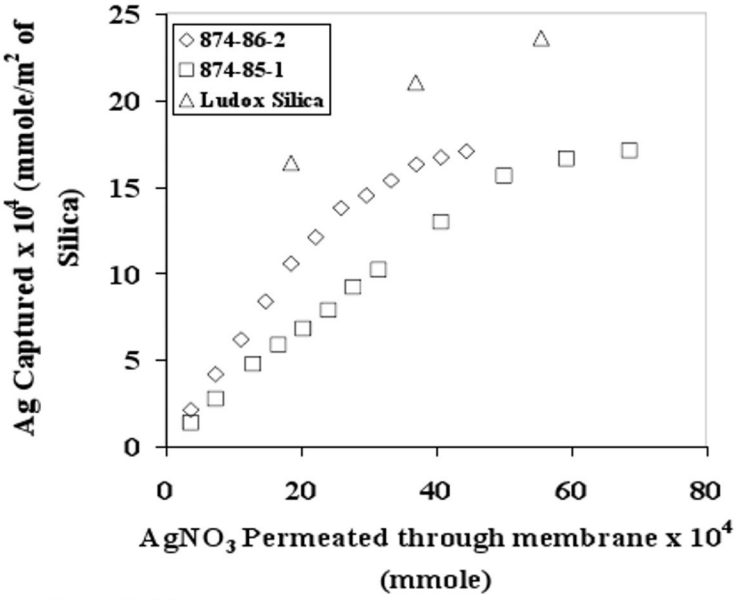

Figure 6. (a)

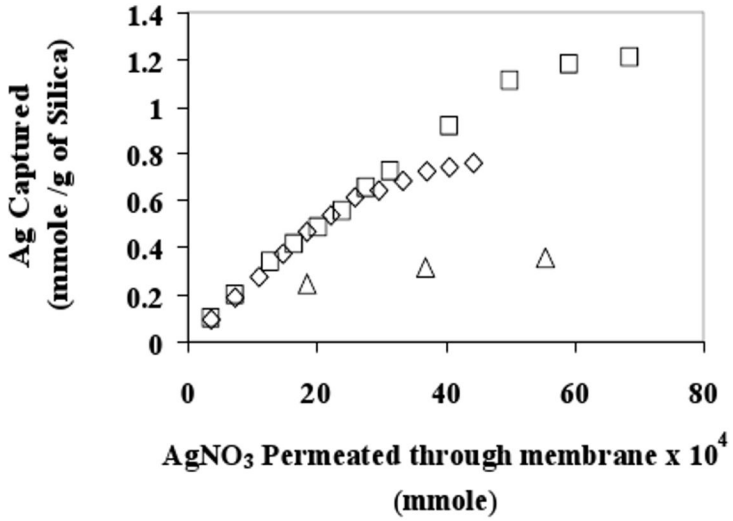

Figure 6. (a) Silver capture with different functionalized silica-cellulose acetate mixed matrix membrane (10% silica loading). Effect of total surface area and accessibility of surface −SH groups on silver ion capture capacity. (b) Silver capture data reported per gram of silica

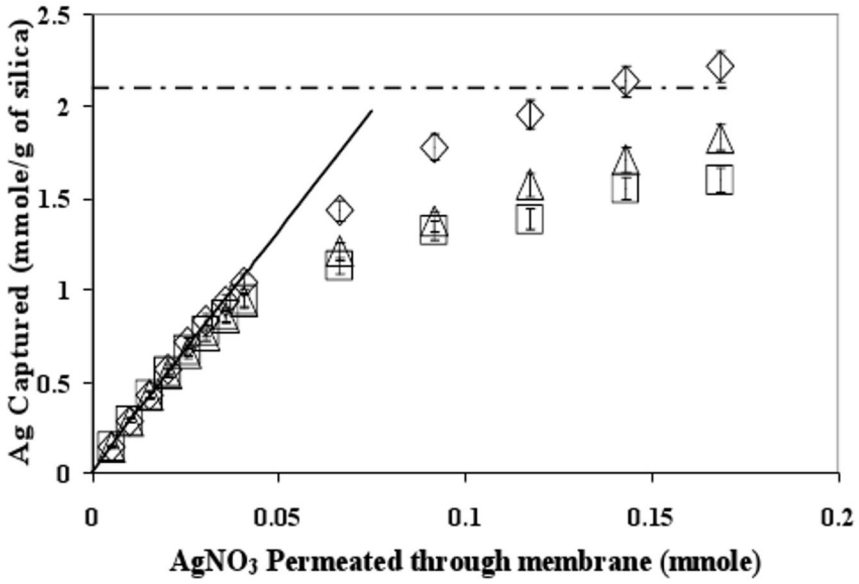

Figure 7. (a)

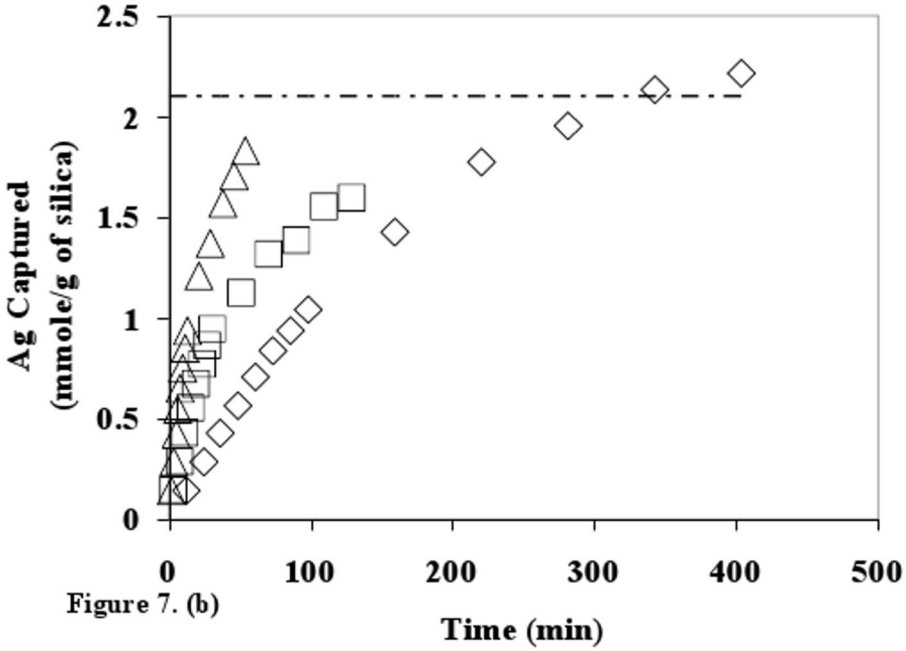

Figure 7. (b)

Figure 7. (a) Effect of residence time (t_R) on silver capture capacity for 40% MPTMS functionalized 874-85-1 silica - polysulfone mixed matrix membrane. The error bars indicate analytical error of measurement for Ag^+ concentration. Solid line ideal case of silver capture. (b) Silver capture data reported as a function of time. Dotted line indicates maximum silver capture capacity

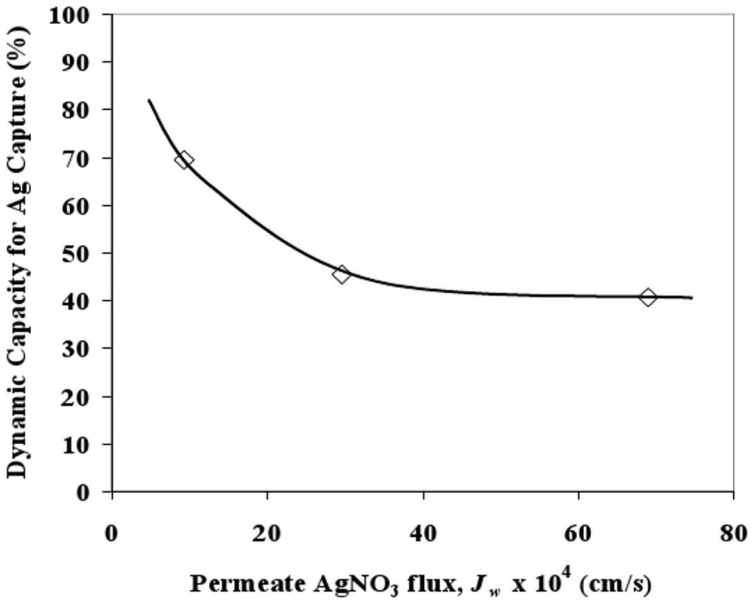

Figure 8. Dynamic silver capture capacity at varying $AgNO_3$ permeate flux with 40% 874-85-1 MPTMS functionalized silica polysulfone MMM. Solid line shows the trend in the data

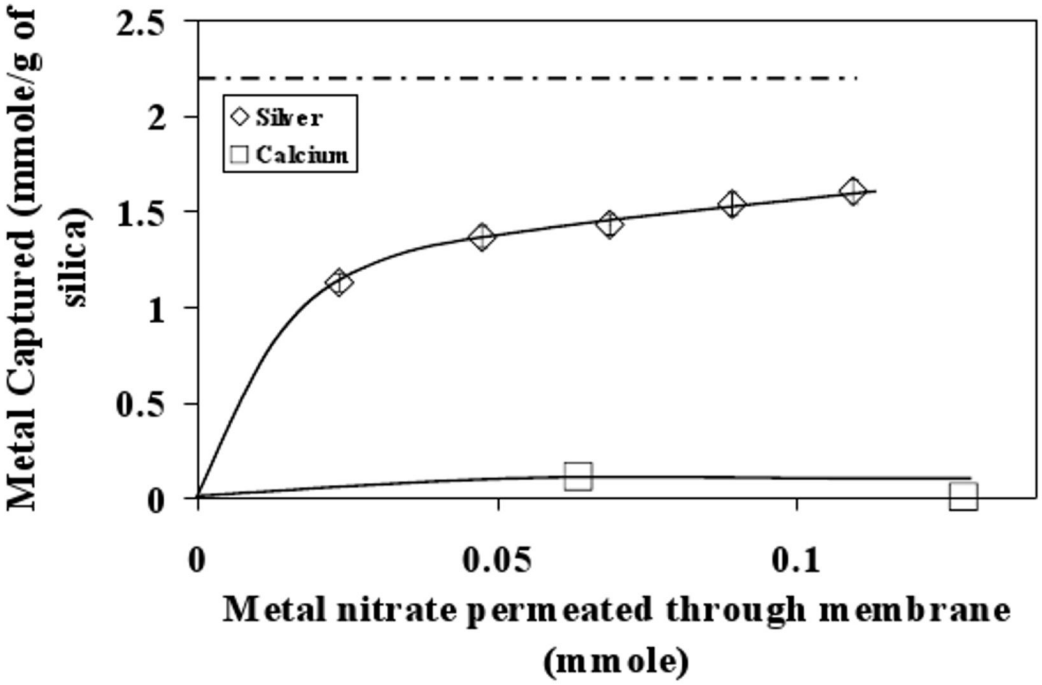

Figure 9. Selectivity towards metal ion capture between Ag^{+} and Ca^{2+} with 30% 874-85-1 MPTMS functionalized silica-polysulfone membrane. The dotted line indicates maximum Ag^{+} capture by functionalized silica particles from Ag^{+} solution. Error bars indicate analytical error of measurement for Ag^{+} concentration. Solid lines show trends in the data

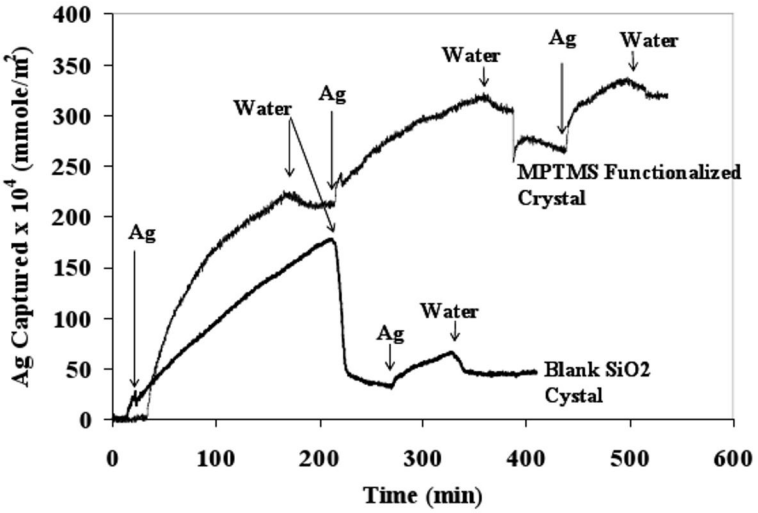

Figure 10. Interaction of Ag^+ with surface −SH groups of MPTMS functionalized quartz crystal by Quartz crystal microbalance. The arrows indicate the time at which the feed solution is changed from water to silver solution or vice a versa

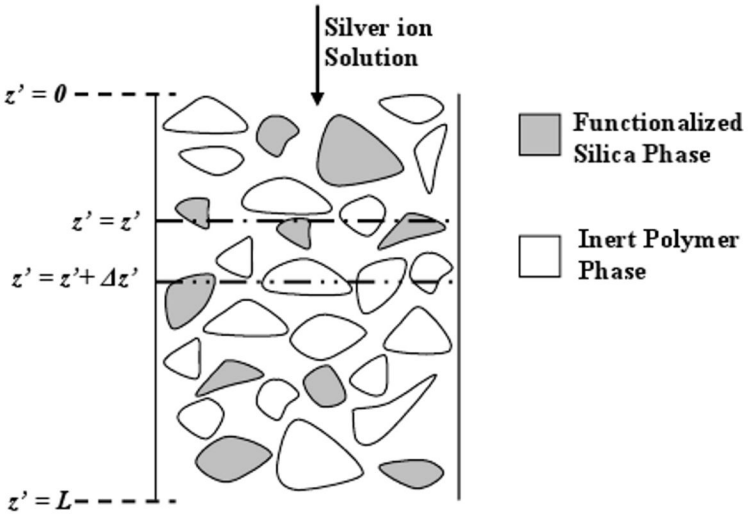

Figure 11. Schematic representation of MMM for modeling purpose

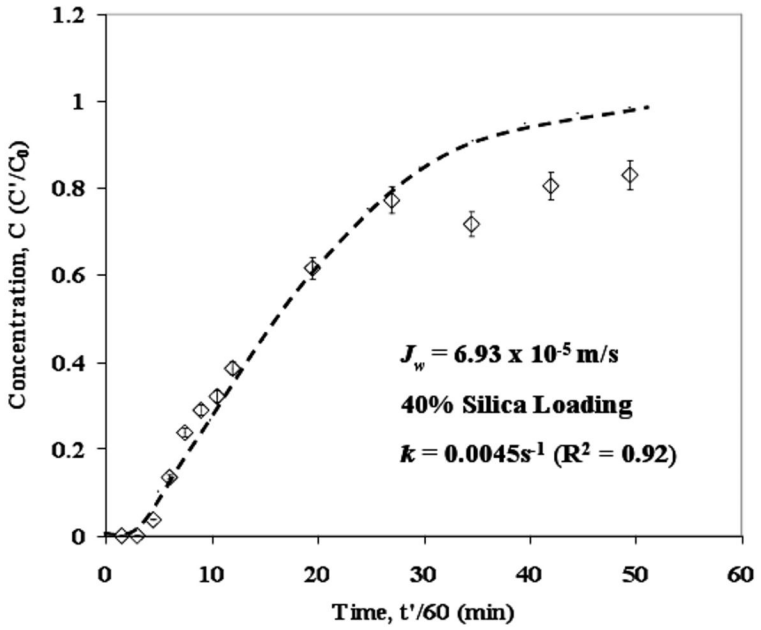

Figure 12. Comparison of experimental and predicted data for 874-85-1 MPTMS functionalized silica-polysulfone MMM silver breakthrough curve. Error bars indicate analytical error of measurement for Ag^+ concentration. Dotted line represents predicted data

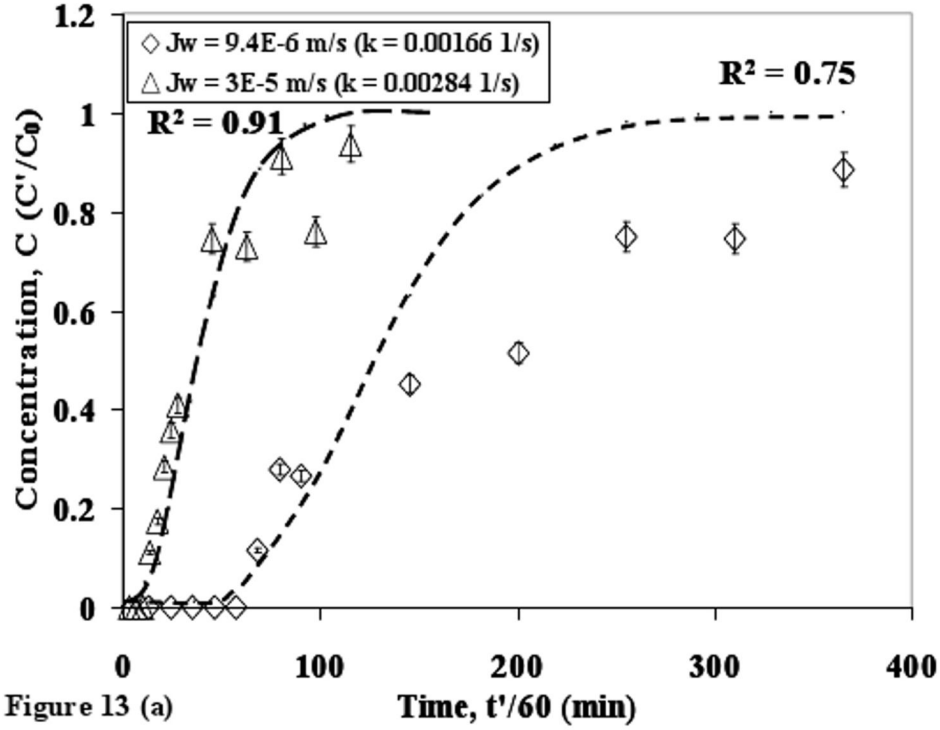

Figure 13 (a)

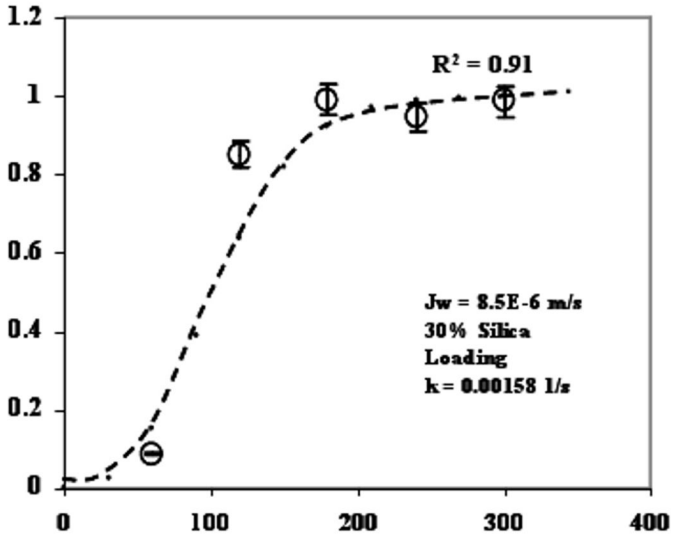

Figure 13 (b)

Figure 13. (a) Comparison of experimental and predicted data for silver breakthrough curves using thiol functionalized 874-85-1 silica-polysulfone MMM with 40% Silica Loading. (b) Data comparison for silver capture with 30% silica loading MMM. In all these cases, no adjustable parameter was used to predict the data. The volumetric mass transfer coefficient (*k*) is obtained from correlation based of membrane flux (J_W). Error bars indicate analytical error of measurement for Ag^+ concentration. Dotted lines show predicted data

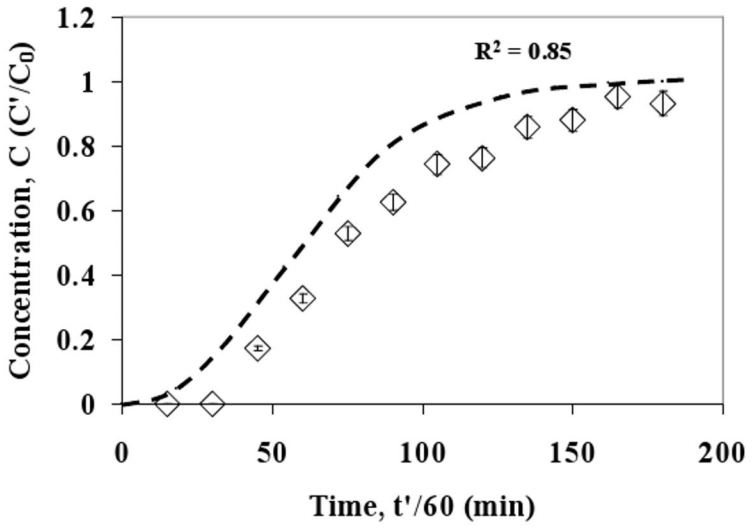

Figure 14. Comparison of experimental and predicted data (dotted line) for silver breakthrough curve using 40% 874-85-1 MPTMS functionalized silica-polysulfone MMMs in the case of double stack membrane experiment. The k value of 0.00202 1/s is obtained from single stack experiment using equation (7). The silica was functionalized under conditions where MPTMS was limiting reactant so as to deliberately achieve lower silver capture capacity (γ = 1880.3 as compared to 5021.8 in previous single stack cases). Error bars indicate analytical error of measurement for Ag^+ concentration

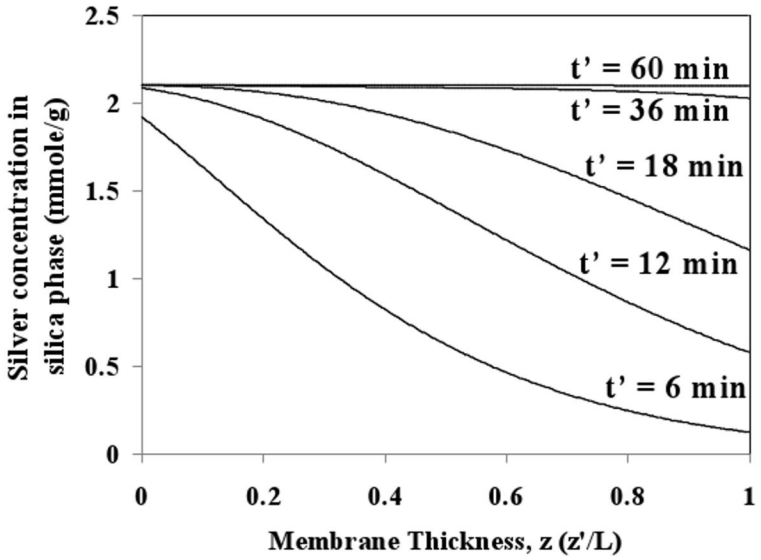

Figure 15. Predicted concentration of silver in silica phase along the membrane thickness at varying times. Feed is 100 mg/L aqueous silver ion solution at transmembrane pressure of 8.2 bar (Residence time, t_R = 2.8 s)

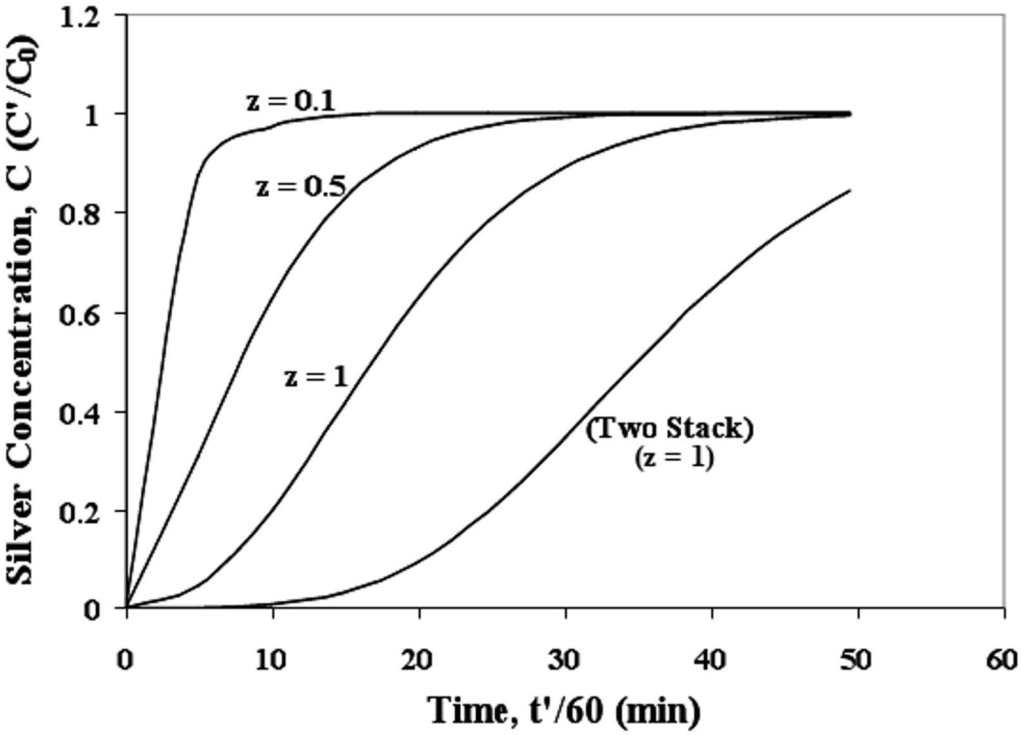

Figure 16. Predicted concentration profile of liquid phase silver concentration at varying membrane thickness. Two stack represents concentration profile for silver capture experiment using two membranes stacked together

Table 1
Characteristics of various types of silica used in this study

	Huber 874-86-2	Huber 874-85-1	Ludox TM 50
Average Particle Size (μm)	3.7	3.3	0.022
Pore Diameter (nm)	11.8	3.54	N/A
BET Surface Area (m^2/g)	444	708	95